Journal of Applied Research in Chemistry

Volume2, Issue2 (Serial: 6), summer 2021

https://science-journals.ir

Adsorption of reactive red 120 dye on modified Fe3O4/SiO2 nanoparticles using (3–Amino propyl) triethoxysilane

Tayebe Pourshamsi[1], Ghodratollah Absalan, Morteza Akhond

Professor Massoumi Laboratory, Department of Chemistry, College of Sciences, Shiraz University, Shiraz 71454, Iran

ABSTRACT

Adsorption of reactive red 120 (RR–120) on Fe_3O_4 magnetic nanoparticles coated by silica which were modified by 3–aminopropyl triethoxysilane is described. Results indicated that the nanoparticles were able to remove about 98% of RR–120 (20.0 mg L^{-1}) under the optimum conditions of 15.0 mg nanoparticles, pH=3.0, and contact time of 7.0 minutes. Adsorption equilibrium was best fit to the Langmuir adsorption isotherm. The maximum adsorption capacity of the adsorbent was 23.98 mg per gram dye. A pseudo–second order kinetic model exhibited the best fit to the experimental data.

Keywords: 3–Aminopropyl triethoxysilane; Reactive red 120; UV–Vis spectrophotometery; Ferrous oxide magnetic nanoparticles; Removal dye

*Corresponding Author E–mail: tayebepoorshamsi@yahoo.com.

1. Introduction

Many industries in area such as cosmetics, foods, textiles, and plastics widely consume dyes and dye stuffs [1-3]. For instance, azo dyes cover about 70% of dyes used in the textile industry. Wastewater samples of these industries contain dye with other chemical materials, which are hazardous to the environment [1]. Charges of such wastes in water sources cause damage to ecological balance and affect photosynthetic activity [1]. Hence, the presence of these materials in the environmental is problematic as they are not easily degraded by biological means. Because dyes are stable and even potentially carcinogenic and toxic, their existence in the environment poses serious environmental, aesthetical and health difficulties [4].

Various physical [5-7] and chemical [8-10] methods have been applied for the removal of dyes from water and wastewater as well as biological methods [11-14]. Literature review [15-19] shows that physical methods, especially adsorption, are of the most applied techniques for dyes removal. Many researchers prefer adsorption with nano adsorbents due to simplicity, low expense and highly efficient of the corresponding procedures.

Utilization of different nanoparticles, for the removal of pollutants in the environment, have been reported in literature [20-23]. Ionic liquid-modified Fe_3O_4 nanoparticles [24], MgO nanoparticles [3], magnetic-modified multi-walled carbon nanotubes (MMWCNTs) [25], L-arginine-functionalized Fe_3O_4 nanoparticles [26], hollow zein nanoparticles [27], Fe_3O_4 NPs modified with a surfactant cetyltrimethylammonium bromide [28], the combination of Fe_3O_4 and ZnCr- layered double hydroxide [29], Fe_3O_4/MgO nanoparticles [30] and $CoFe_2O_4$ nanoparticles [31] are some examples.

Magnetic nanoparticles (MNPs) have provided wide applications in variety of fields including magnetic fluids [32], catalysis [33, 34], biotechnology [35], magnetic resonance imaging [36, 37], data storage [38], environmental remediation [39, 40] and sensors and biosensors construction [41]. These are due to their unique properties such as, good biocompatibility, powerful super paramagnetism, low toxicity, facile preparation and high adsorption ability [41]. Moreover, they have high surface areas with low mass transfer

resistance [41]. Co–precipitation is their convenient synthesis method from aqueous Fe(II)/Fe(III) solutions by adding a basic compound under an inert atmosphere [42]. A stoichiometric ratio of 2:1 for Fe(III):Fe(II) is important in their synthesis [43, 44].

To prevent accumulation of Fe_3O_4 magnetic nanoparticles and improve their chemical stability in aqueous solutions, an inert silica layer is usually coated on their surface [45]. The Stober process [46], which comprises hydrolysis and ploy–condensation of tetraethoxysilane in ethanol [45], is one of the methods of choice for coating purposes.

Functional groups are tailored around MNPs for specific tasks which can be anchored as an organic molecule shell such as aminopropyltriethoxysilane (APTES) [47]. It modifies the surface of the nanoparticles through the attachment of aminopropylsilane groups $(–O)_3Si–CH_2–CH_2–CH_2–NH_2$ via formation of covalent bonds which are bound to the particle surface [48].

The aim of this research was to use surface–modified magnetic nanoparticles for removal and preconcentration of reactive red 120. To do this, 3–aminopropyl triethoxysilane (APTES) was used as a chemically–bounded modifier, which improve reusability and stability of the adsorbents. The effects of different parameters, such as dosage of Fe_3O_4/SiO_2/APTES nanoparticle, pH of the aqueous sample, contact time of the reagents, solvent effect, temperature, ionic strength and comparative attempt among the building constituents of the adsorbent have been evaluated. Reactive red dyes contain both anionic and cationic sites such as hydroxylates, sulfonates, and chloride [24]. Some characteristics of reactive red 120 dye are reported in Table 1.

2. Experimental

2.1. Reagents and solutions

Analytical grades reactive red 120 (RR–120), sodium hydroxide solution (1.5 mol L^{-1}), hydrochloric acid (37.0%, w/w), $FeCl_3.6H_2O$ (96.0%, w/w), $FeSO_4·7H_2O$ (99.9 %w/w), ethanol (96.0%), tetraethyl orthosilicate (TEOS), 3-aminopropyltriethoxysilane (APTES), and ammonia were purchased from Merck (Darmstadt, Germany). Stock

Solution (1000.0 mg L^{-1}) of RR–120 dye was prepared. The pH adjustments were performed with HCl and NaOH solutions.

2.2. Apparatus

A spectrophotometer Model Pharmacia Ultraspec 4000 was used for recording the UV–Visible spectra and absorbance measurements by using 1.0–cm quartz cells. The sizes of Fe_3O_4, Fe_3O_4/SiO_2 and Fe_3O_4/SiO_2/APTES nanoparticles were determinated with scanning electron microscope (KYKY–EM3200). The XRD measurements were performed on an XRD Bruker D8 Advance. A Shimadzu FTIR 8300 spectrometer was used for recording the FTIR spectra. A Metrohm 780 pH meter was used for measuring the value of pH. For dispersing nanoparticles in solution, an ultrasonicator (Model CD–4800, China) was used and for collecting nanoparticles from solution, a super magnet Nd–Fe–B (1.4 T, 10× 5× 2 cm made in China) was used. All measurements were performed at ambient temperature.

2.3. Fabrication of Fe_3O_4/SiO_2/APTES nanoparticles

The nanoparticles of Fe_3O_4 were prepared by co–precipitating Fe(II) and Fe(III) ions with a molar ratio of about 0.5 in sodium hydroxide solution (1.5 mol L^{-1}) with a stirring rate of 2000 rpm for 30 min at room temperature [49].

The Fe_3O_4 nanoparticles were coated with silica by a sol-gel process reported in the literature [50]. Briefly, 0.1 g magnetic nanoparticles and 100.0 mL ethanol were mixed and were ultrasonicated for about 30.0 min. Then, under mechanical stirring, 0.5 mL of TEOS was added and the mixture was adjusted to pH 11.0 with ammonia solution and was refluxed at 130 ^{0}C for 24.0 h. The Fe_3O_4/SiO_2 nanoparticles were collected with a permanent magnet and were thoroughly washed with ethanol for several times and were eventually kept at 40 ^{0}C for 24.0 h for drying purpose [50]. The Fe_3O_4/SiO_2 nanoparticles were dispersed by ultrasonication for 30.0 min in ethanol. The concentration of the Fe_3O_4/SiO_2 nanoparticles was adjusted to 0.1 g/100 mL and then 0.1 mL 3–aminopropyltriethoxysilane (APTES) was added to the solution. The mixed solution was heated to 130 ^{0}C for 7.0 h. The Fe_3O_4/SiO_2/APTES nanoparticles were collected with a permanent

magnet and were thoroughly washed with ethanol for several times, and were dried at 40 ^{0}C for 24 h [50].

For synthesis of Fe_3O_4/APTES, part of Fe_3O_4 nanoparticles (0.0128 M) were dispersed in ethanol. An aliquot of 25 ml of this solution was diluted to 150 ml by ethanol and 1 ml H_2O. This mixture was ultrasonically treated for 30 min. Then 35 ml of 3-aminopropyltriethoxysilane was added while stirring for 7 h. The resulted product was washed 5 times with ethanol and then dried at room temperature under vacuum to be obtained in a powdered form [51].

2.4. Procedure of adsorption of dyes

To study the effect of the experimental parameters, the batch technique was conducted. Aliquots of 6.0 mL of the dye solution with initial concentrations of 20–50 mg L^{-1} in the pH range of 1.0–12.0, adjusted by 0.l0 mol L^{-1} HCl and NaOH solutions, were prepared and transferred into individual beakers. A known dosage of Fe_3O_4/SiO_2/APTES, in the range of 5–30 mg, was added to each solution and the suspensions were immediately stirred with a magnetic stirrer for a predefined period of time (in the range of l–30 minutes). After the mixing time elapsed, the Fe_3O_4/SiO_2/APTES nanoparticles were magnetically separated and the aqueous phase was analyzed for the residual dye. The percent adsorption of dye, i.e. the dye–removal efficiency of Fe_3O_4/SiO_2/APTES, was determined by using the following equation (Eq.1):

(1) $\%\text{Removal} = \frac{(C_0 - C_f)}{C_0} \times 100$

where C_o and C_f (mg L^{-1}) represent the initial and final (after adsorption) dye concentrations, respectively. All experiments were performed at ambient temperature.

2.5. Procedure of adsorption isotherms of dyes

Adsorption isotherms present information on how an adsorption system proceeds and show how efficiently a given adsorbent interacts with adsorbate [52]. Among several isotherm models [53-57], the most common models used to investigate the adsorption isotherms are Langmuir and Freundlich. Experiments for the estimation of the

individual adsorption isotherms of reactive red 120 (RR–120) onto Fe_3O_4/SiO_2/APTES surface were performed by adding various amounts of Fe_3O_4/SiO_2/APTES, in the range of 5.0–30.0 mg, to a Series of beakers containing 6.0 mL of 45.0 mg $L^{-1}$of the dye solution at pH 3.0. The solutions were stirred for 7 minutes at 25 °C to attain the equilibrium condition. The aqueous phases were tested for the residual dye after settlement of the nanoparticles. The amount of the dye adsorbed onto Fe_3O_4/SiO_2/APTES was calculated based on the following mass balanced equation (Eq.2):

$$q_e = \frac{(C_0 - C_e)V}{m} \quad (2)$$

Where q_e (in mg g^{-1}) is the adsorption capacity (mg adsorbate adsorbed onto the gram amount of adsorbent), C_0 and C_e (in mg L^{-1}) are the initial and equilibrium adsorbate concentrations, respectively; V (in L) is the volume of the adsorbate solution, and m (in g) is the mass of adsorbent added.

2.6. Procedure of adsorption kinetics of dyes

To study the adsorption kinetics of dyes, the Fe_3O_4/SiO_2/APTES (15 mg) was incubated with 6.0 mL of the sample solution (pH 3.0), containing 30.0 mg $L^{-1}$of dye, and the suspension was immediately stirred (1000 rpm) for different periods of time. Adsorption kinetic data were obtained by measuring the concentration of dye in the mother liquor at different times after removing the Fe_3O_4/SiO_2/APTES nanoparticles.

3. Results and discussion

3.1. Characterization of Fe_3O_4/SiO_2/APTES nanoparticles

The particle size of Fe_3O_4, Fe_3O_4/SiO_2 and Fe_3O_4/SiO_2/APTES nanoparticles were determined by scanning electron microscopy (SEM). Fig.1a shows the SEM images of the synthesized Fe_3O_4 nanoparticles. The particles had a narrow size distribution with an average particle diameter of ~20 nm. Fig.1b shows the SEM images of the synthesized Fe_3O_4/SiO_2 nanoparticles. These nanoparticles had a narrow size distribution with an average diameter of ~83 nm. Fig.1c

shows the SEM images of the synthesized Fe_3O_4/SiO_2/APTES having a narrow size distribution with an average diameter of 87 nm.

The peaks positions and relative intensities observed in XRD patterns of Fe_3O_4, Fe_3O_4/SiO_2 and Fe_3O_4/SiO_2/APTES nanoparticles are shown in Fig.2 for comparison. Five characteristic peaks for Fe_3O_4, Fe_3O_4/SiO_2 and Fe_3O_4/SiO_2/APTES (2θ = 30.3, 35.75, 43.3, 57.76 and 63.5), corresponding to indices (220), (311), (400), (511) and (440) are shown in the pattern [58]. Although the Fe_3O_4/SiO_2 nanoparticles were coated with TEOS and APTES, the analysis of XRD patterns indicated very distinguishable peaks for magnetite crystal [59]. The data indicated that heating in an ethanol bath for 7 h, during the silanization reaction, had not affected the physical characteristics of the magnetic nanoparticles [59, 60].

The FTIR spectra of Fe_3O_4, Fe_3O_4/SiO_2 and Fe_3O_4/SiO_2/APTES nanoparticles are shown in Fig.3. In the case of Fe_3O_4, Fig.3a, the broad absorption band at 3440 cm^{-1} indicated the presence of surface hydroxyl groups (O–H stretching) and the bands at $\leq$700 cm^{-1} were related to vibrations of the Fe–O bonds [58]. The presence of magnetic nanoparticles can be proven by the appearance of two strong absorption bands around 632 and 570.9 cm^{-1}. The Fe–O bond of the bulk magnetite was observed at 570.9 cm^{-1} [58, 61]. As can be seen from Fig.3b, in addition to the magnetic peaks, the OH stretching vibrations of Si–OH group were observed at 1072.3 cm^{-1} [62]. Vibrations for Si–OH and Si–H were observed at 830 cm^{-1}comprising a chemical bound of TEOS to the magnetic nanoparticles [62]. As can be seen from Fig.3c, in addition to the Fe_3O_4/SiO_2 peaks, asymmetric and symmetric stretching of Si–O–Si vibrations were also observed at 1064.6 cm^{-1} and 830 cm^{-1}, respectively. Alkyl C–H stretching and bending vibrations appeared at 2923.9 cm^{-1} and 1542.9 cm^{-1}, respectively. Thus, the peaks at 2923.9 cm^{-1} and 1542.9 cm^{-1} are assigned to $–CH_2$ stretching and bending vibrations, respectively. The N–H and C–N stretching were observed at 3741.6 cm^{-1} and 1635.5 cm^{-1}, respectively. The existence of the $–CH_2$ and $–NH_2$ groups indicated that the surfaces of the silica–coated magnetic nanoparticles were modified with APTES [62].

The experimental curves corresponding to the pH drift method [63] were obtained for Fe_3O_4, Fe_3O_4/SiO_2 and Fe_3O_4/SiO_2/APTES

nanoparticles and are reported in Fig.4. Suspensions of 5.5 g L^{-1} of individual nanoparticles were prepared and were brought into contact with 0.10 mol L^{-1} NaCl to be adjusted in the pH of 2.0-12.0. Nitrogen gas was bubbled through the solution at 25 ^{0}C in order to remove carbon dioxide off the solution and stabilize the initial pH value. The suspensions were agitated for 48 hours to achieve an equilibrium pH value. The pH at the point of zero charge (pH_{pzc}) was obtained by plotting the difference of the final and initial pHs (ΔpH) versus the initial pH. As it is shown in Fig.4, the pH_{pzc} values for Fe_3O_4 nanoparticles was 6.5, for Fe_3O_4/SiO_2 nanoparticles was 7.5 and for Fe_3O_4/SiO_2/APTES nanoparticles was 6.0. These data showed that a negative zeta potential was developed by silica coating at pH values higher than 7.5 which shifted to pH 6.0 after being modified by amino functionality [50].

3.2. Dye adsorption

The efficiencies of the prepared Fe_3O_4, Fe_3O_4/SiO_2 and Fe_3O_4/SiO_2/APTES as adsorbents for removal of RR–120 from aqueous solutions were investigated. Preliminary tests were carried out to investigate parameters such as nanoparticles dosage, pH of the solution, contact time between reagents, ionic strength and temperature of the solutions. Results are discussed in the following sections.

3.2.1. Effect of solution pH and adsorption capacity of nanoparticles

The dye solution pH alters the surface charges of the nanoparticles as well as changing the degree of ionization of the dye; therefore, it is important to be investigated. The influence of pH on adsorption of RR–120 onto Fe_3O_4/SiO_2/APTES surface was assessed in the pH range of 0.5 to 12.0 and the corresponding results are shown in Table 2. The initial concentrations of the dye and adsorbent dosage were set at 20 mg L^{-1} and 20.0 mg, respectively, with a stirring time of 10 min. The results indicated that there was a decrease in percent removal of dye as pH increased to values more than 3.5. Generally, the higher adsorption of dye at pH 3.0 could be due to the electrostatic attractions between the anionic forms of the dye and positively-charged

nanoparticles. At higher pH values, the abundance of OH^- is expected to prevent the adsorption of the anionic forms of the dye molecules [24].

The adsorption capacities of Fe_3O_4, Fe_3O_4/SiO_2, Fe_3O_4/APTES, and Fe_3O_4/SiO_2/APTES nanoparticles for dyes were tested in the pH range of 0.5 to 12.0. The results, shown in Fig.5, indicated that at low pH values, Fe_3O_4 nanoparticles dissolved as reported by Zargar et al. [64]. The same situation was also observed for dissolution of Fe_3O_4/APTES nanoparticles at low pH values. To overcome this problem, for both Fe_3O_4 and Fe_3O_4/APTES nanoparticles, the surface of Fe_3O_4 nanoparticles were coated with TEOS [65]. Fig.5 shows a comparative attempt among the building constituents of the adsorbents revealing that their adsorption capacities for reactive red 120 were in the following order: Fe_3O_4/SiO_2/APTES > Fe_3O_4/APTES > Fe_3O_4/SiO_2 > Fe_3O_4. Accordingly, Fe_3O_4/SiO_2/APTES nanoparticles, as suitable adsorbents for RR–120 dye, were used in this study.

3.2.2. Effect of nanoparticles dosage

Capacity factor of the adsorbent is a dosage of adsorbent required for adsorbing a given initial concentration of the adsorbate. To find this, the dosage of Fe_3O_4/SiO_2/APTES for removal of RR–120 was investigated using a batch technique by adding a certain value of the adsorbent, in the range of 5.0–30.0 mg of its dried powder form, into individual beakers containing 6.0 mL of the dye solution. The initial dye concentration and the pH of its aqueous solution were fixed at 20 mg L^{-1} and 3.0, respectively. Each resulting suspension was immediately stirred for 10.0 minutes. After elapsing the mixing time, the Fe_3O_4/SiO_2/APTES nanoparticles were magnetically separated and the solution was analyzed for the residual dye. According to Table 2, removal of the dye increased with increasing Fe_3O_4/SiO_2/APTES dosage up to a value of 15.0 mg and reached ~ 98% at this dosage. This observation can be explained due to the presence of huge numbers of adsorption sites on the nanoparticles surface for adsorption of dye molecules when higher dosage of Fe_3O_4/SiO_2/APTES was used. Hence, the optimum dosage of

Fe_3O_4/SiO_2/APTES powder for removing 0.12 mg of RR–120 was found to be 15.0 mg.

3.2.3. Effect of contact time

The contact time between the reagents, i.e adsorbent and adsorbate, is one of the most important parameter that affect the efficiency of the adsorption processes. Short adsorption equilibrium contact time favors the application of the adsorption process, for example, for the Economical wastewater treatment. The effect of contact time (also called stirring time) on the performance of Fe_3O_4/SiO_2/APTES in adsorbing RR–120 was investigated. The solution pH and Fe_3O_4/SiO_2/APTES dosage were fixed at 3.0 and 15.0 mg, respectively, for all batch experiments. The initial dye concentration of all test solutions was 20 mg L^{-1}. According to Table 2, adsorption was happened immediately by adding Fe_3O_4/SiO_2/APTES powder to the dye solution. The removal efficiency for RR–120 rapidly increased by increasing the stirrer time. When the stirring reached to 7.0 minutes, the removal efficiency value was 98%. Therefore, the optimum contact time was considered to be 7.0 minutes for RR–120 removal at the optimum experimental conditions.

3.2.4. Effect of ionic strength of solution

The effect of solution ionic strength on removal of RR–120 was investigated under optimum experimental conditions in a batch technique (Table 2). A selected concentration of KCl, in the range of 0.0–1.0 mol L^{-1}, was added to individual beakers containing 6.0 mL of the tested dye solution with a concentration of 20.0 mg L^{-1}. The solution pH and Fe_3O_4/SiO_2/APTES dosage were fixed at 3.0 and 15.0 mg, respectively, and the stirring time was 7.0 min. After the mixing time elapsed, the Fe_3O_4/SiO_2/APTES nanoparticles were magnetically separated and the solution was analyzed for the residual dye. The Fe_3O_4/SiO_2/APTES nanoparticles had removed ~ 98% of RR–120 at various concentration of KCl (0.0–1.0 mol L^{-1}). This showed that dye removal was due to hydrophobic interaction between Fe_3O_4/SiO_2/APTES nanoparticles and the day molecules. It is known that in the presence electrostatic interactions, the adsorption could be decreased by increasing ionic strength [66].

3.2.5. Effect of solution temperature

It is important to investigate the effect of temperature on adsorption from the practical point of view. The effect of temperature on the adsorption of RR–120 on Fe_3O_4/SiO_2/APTES nanoparticles was investigated at initial dye concentration of 20.0 mg L^{-1}. The solution pH and Fe_3O_4/SiO_2/APTES dosage were fixed at 3.0 and 15.0 mg, respectively, and a stirring time of 7.0 minutes was used. The results (Table 2) indicated that solution temperature, in the range of 283 to 308 K, had no significant effect on removal of RR–120.

3.2.6. Effect of solvent on adsorption of reactive red 120

The effects of four selected solvents on the adsorption of RR–120 onto Fe_3O_4/SiO_2/APTES nanoparticles were investigated in a batch mode. They were distilled water, mixture of 50% (v/v) of ethanol and distilled water, mixture of 50% (v/v) of acetone and distilled water, and mixture of 50% (v/v) of DMSO and distilled water. The solution pH and Fe_3O_4/SiO_2/APTES dosage were fixed at 3.0 and 15.0 mg, respectively. The initial dye concentration for all test solutions was 20.0 mg L^{-1}. The individual test solutions were prepared in different solvents as mentioned above. Table 3 shows the removal efficiencies of dye when different solvents were used. These data indicated that percent adsorption in water was about 98%, which was the highest when compared to other solvents. By using an organic/water mixture, the tendency of nanoparticles toward adsorption of dye decreased revealing that the dye removal could be due to strong hydrophobic interaction between nanoparticles and the dye. This also proved when the effect of ionic strength was studied in the previous section. The lower hydrophobic character of a solvent provides higher interaction between the dye and the nanoparticles. As it is shown in Table 3, in 50% (v/v) ethanol/ water with a lower hydrophobicity, the adsorption of dye molecules onto nanoparticles was more than in 50% (v/v) acetone/water with a higher hydrophobicity. Dimethylsulfoxide is a polar aprotic solvent that dissolves both polar and nonpolar compounds, so as was expected, the adsorption of dye molecules in 50% (v/v) DMSO/water, with a lower hydrophobicity, was higher than in 50% (v/v) acetone/water.

3.2.7. Stability of the adsorbed dye

The Fourier transform infrared spectra of dye molecule as well as the dye molecules adsorbed onto Fe_3O_4/SiO_2/APTES nanoparticles are shown in Fig.6. For the free reactive red 120 dye, the peaks at 1312 and 1496 cm^{-1} correspond to the benzene ring; the broad peak at 3440.8 cm^{-1} is representative of N–H stretching of the aromatic amine. The peak at 1041.5 cm^{-1} is attributed to the phenolic OH groups and the peaks at 1196.8 and 1635.5 cm^{-1} indicate the aromatic C–O and –N=N– stretching of the azo group, respectively. The peak at 1114 cm^{-1} represents the signature of the C–N–C [67].

In the case of RR–120 dye adsorbed onto Fe_3O_4/SiO_2/APTES nanoparticles, when compared with free Fe_3O_4/SiO_2/APTES nanoparticles (explained in section 3.1), new peaks were observed in 1324.9, 1456.3, 1511.9 and 1586.5 cm^{-1} showing that RR–120 was adsorbed onto the surface of nanoparticles [67]. The observed shift in the position of these peaks, compared with free RR–120, indicated to the attachment of dye onto Fe_3O_4/SiO_2/APTES nanoparticles surface. These results proved that the dye had been adsorbed onto the surface of nanoparticles without being degraded.

3.3. Adsorption isotherm modeling

The equilibrium adsorption data of RR–120 on the Fe_3O_4/SiO_2/APTES nanoparticles surface was analyzed using Langmuir and Freundlich models. The models fit to equilibrium adsorption data of the dye was evaluated by the correlation coefficients (R^2) of the linear regression plots. The fitting of the obtained experimental data to both models was tested and the resulting plots are shown in Fig.7. Table 4 summarizes the models constants and their corresponding correlation coefficients. As shown in Table 4, the R^2 of the Langmuir model was higher for the adsorption of RR–120 indicating that the Langmuir adsorption isotherm more accurately described the adsorption of RR–120 onto Fe_3O_4/SiO_2/APTES nanoparticles. This in turn suggested that adsorption occurred as monolayer deposition of dye [55]. Also, as seen in Table 4, the maximum adsorption capacity of Fe_3O_4/SiO_2/APTES nanoparticles for adsorption of RR–120 was found to be 23.98 mg g^{-1}.

3.4. Adsorption kinetic modeling

Plots of experimental results of RR–120 fitted to the pseudo–first– and pseudo–second–order reaction rate models are shown in Fig.8. Table 5 gives a summary of the models and their corresponding constants along with the correlation coefficients for the linear regression plots of the tested dye. As shown in Table 5, higher values of R^2 was obtained for pseudo–second order adsorption rate model indicating that the adsorption rate of dye onto Fe_3O_4/SiO_2/APTES Nanoparticles can be properly explained using the pseudo–second order rate.

3.5. Desorption and reusability studies

The reusability and regeneration of an adsorbent are important parameters to be reported. Possible desorption of RR–120 was tested by using different solutions such as pure acetone, pure ethanol, 1.0 mol L^{-1} sodium chloride aqueous solution (NaCl (aq)), and NaCl (aq): acetone (with volume ratios of 1:1, 2:1 and 1:2). The study revealed that the adsorbed RR–120 molecules could be completely desorbed in the presence of mixed NaCl (aq) : acetone with a volume ratio of 2:1 [24]. In this study, more than 98% of the adsorbed dye could be desorbed and recovered by 3.0 mL of NaCl (aq): acetone with a volume ratio of 2:1 when 0.12 mg dye (6.0 mL of dye with a concentration of 20.0 mg L^{-1}) was already adsorbed onto Fe_3O_4/SiO_2/APTES nanoparticles surface. The results showed that the desorption process was quantitative after recycles the desorbing solution for four times.

The reusability of the adsorbents in several consecutive separation processes was tested and the results showed that Fe_3O_4/SiO_2/APTES nanoparticles can be reused for 3 times after being recycled each time with insignificant reduction in their removal efficiency. The stability of Fe_3O_4/SiO_2/APTES nanoparticles after storing the dried particles at room temperature was tested for adsorption of RR–120. The results indicated that APTES was stable for a period of 1 month at the surface of Fe_3O_4/SiO_2.

4. Conclusion

The Fe_3O_4/SiO_2/APTES nanoparticles were produced and tested as adsorbents for the removal of RR–120 dye. Results indicated that the synthesized nanoparticles could effectively remove RR–120 in a short period of 7.0 min. Experimental results revealed that the Fe_3O_4/SiO_2/APTES nanoparticles had removed ~ 98% (RSD =2.8%) of dye under the optimum operational conditions. The dosage of nanoparticles and pH of the sample solution were obtained to be 15.0 mg and 3.0, respectively, while a stirring time of 7.0 minutes was used. A comparative attempt among the building constituents of the adsorbent revealed that their adsorption capacities for reactive red 120 were in the following order: Fe_3O_4/SiO_2/APTES > Fe_3O_4/APTES > Fe_3O_4/SiO_2 > Fe_3O_4. The maximum adsorption capacity of Fe_3O_4/SiO_2/APTES was 23.98 mg per gram reactive red 120. Isotherm modeling revealed that the Langmuir equation could better describe the adsorption of RR–120 onto Fe_3O_4/SiO_2/APTES nanoparticles. Kinetic data were significantly fitted to the pseudo–second–order adsorption. The dye removal could be due to hydrophobic interaction rather than electrostatic interaction between Fe_3O_4/SiO_2/APTES nanoparticles and the dye. In addition, NaCl (aq): acetone solution was suitable for desorption of RR–120 and the reusability of Fe_3O_4/SiO_2/APTES was for three times.

Acknowledgements

The authors wish to acknowledge the support of this work by Shiraz University Research Council.

Journal of Applied Research in Chemistry

Volume2, Issue2 (Serial: 6), summer 2021

https://science-journals.ir

5. Tables

Table 1: Some characteristics of reactive red-120 (RR-120) [24].

Characteristic	
Molecular formula	$C_{44}H_{24}Cl_2N_{14}Na_6O_{20}S$
Dye index name	Reactive Red-120
Molecular weight ($g\ mol^{-1}$)	1470
Water solubility ($g\ L^{-1}$)	7 0
λ_{max} (nm)	530
Class	Diazo(-N=N-bond)
Chemical structure	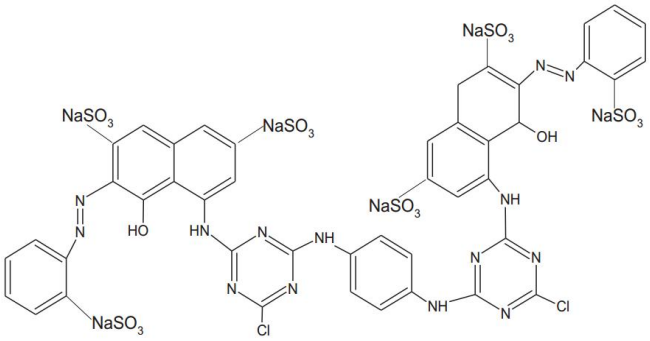

Table 2: Optimization and selection of physical and chemical parameters effecting on adsorption of reactive red 120.

	Parameter	Interval value	Optimum/ selected value
Chemical parameters:	Solution pH	0.5-12.0	3.0
	Ionic strength of solution, KCl (mol L^{-1})[a]	0.0-1.0	0.0
Physical parameters:	Nanoparticles dosage (mg)	5-30	15
	Contact time (min)	1-20	7
	Solution temperature (K)	283-308	Room temperature

a: Calculated based on the concentration of KCl.

Table 3: Effect of solvent on adsorption of reactive red 120 (n=3).

Solvent	Hydrophobic character	Dye removal efficiency (%) ($\pm SD$)
Distilled water	Lowest	98.15 ± 1.32
Ethanol/water (50% v/v)	Lower	90.33 ± 1.02
DMSO/water (50% v/v)	Higher	51.10 ± 2.42
Acetone/ water(50% v/v)	The highest	18.49 ± 1.05

Table 4: Adsorption isotherms parameters of RR-120 onto Fe_3O_4/SiO_2/APTES nanoparticles.

Journal of Applied Research in Chemistry

Volume2, Issue2 (Serial: 6), summer 2021

https://science-journals.ir

Dye	Langmuir model			Freundlich model		
	q_{max} (mg g^{-1})	b (L g^{-1})	R^2	K_F	n	R^2
RR-120	23.98	1.71	0.9978	14.5915	7.2516	0.969 5

Table 5: Adsorption kinetic constants of RR-120 onto Fe_3O_4/SiO_2/APTES nanoparticles.

Dye	Pseudo-first-order model			Pseudo-second-order model		
	k_1 (min^{-1})	q_e (mg g^{-1})	R^2	k_2 (g $mg^{-1}min^{-1}$)	q_e (mg g^{-1})	R^2
RR-120	0.318	2.82	0.9734	0.286	12.28	0.9998

6. Caption and legends for figures

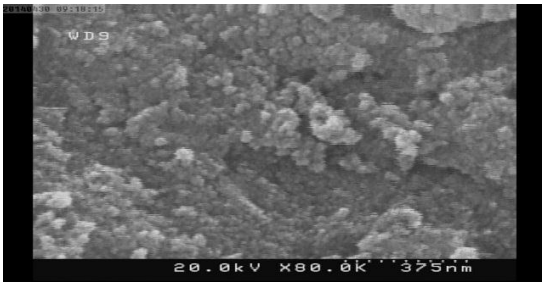

Journal of Applied Research in Chemistry

Volume2, Issue2 (Serial: 6), summer 2021

https://science-journals.ir

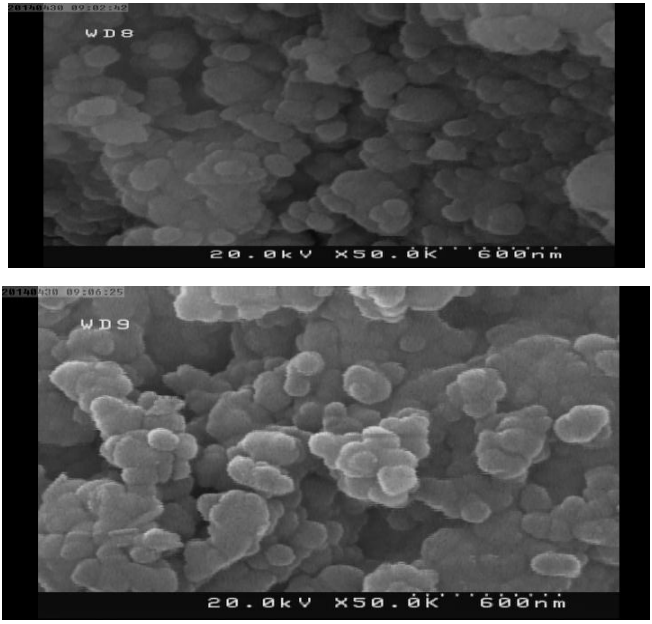

Fig.1: The SEM images of a, Fe_3O_4 nanoparticles; b, Fe_3O_4/SiO_2 nanoparticles; and c, Fe_3O_4/SiO_2/APTES nanoparticles.

Journal of Applied Research in Chemistry

Volume2, Issue2 (Serial: 6), summer 2021

https://science-journals.ir

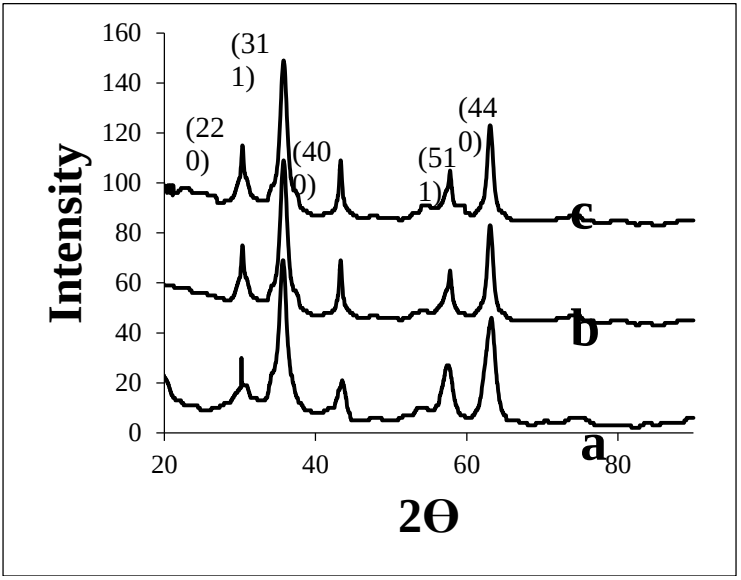

Fig.2: the XRD patterns of a, Fe_3O_4 nanoparticles; b, Fe_3O_4/SiO_2 nanoparticles; and c, Fe_3O_4/SiO_2/APTES nanoparticles.

Journal of Applied Research in Chemistry

Volume2, Issue2 (Serial: 6), summer 2021

https://science-journals.ir

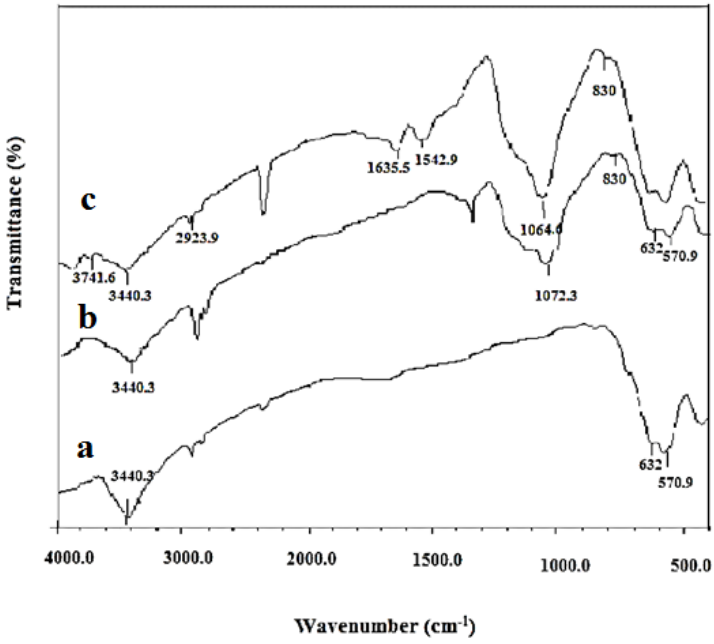

Fig.3: FTIR spectra of a, Fe_3O_4 nanoparticles; b, Fe_3O_4/SiO_2 nanoparticles; and c, Fe_3O_4/SiO_2/APTES nanoparticles.

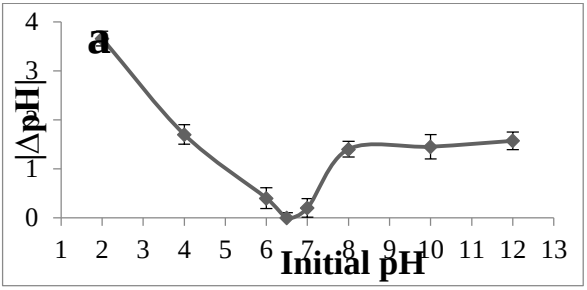

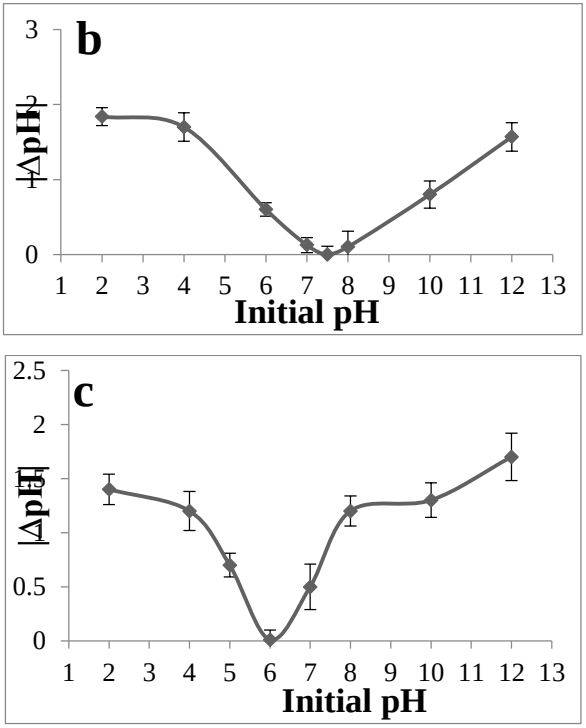

Fig.4: ΔpH versus initial pH for determination of poin of zero charge (pH_{pzc}) of a, Fe_3O_4 nanoparticles; b, Fe_3O_4/SiO_2 nanoparticles; and c, Fe_3O_4/SiO_2/APTES nanoparticles.

Journal of Applied Research in Chemistry

Volume2, Issue2 (Serial: 6), summer 2021

https://science-journals.ir

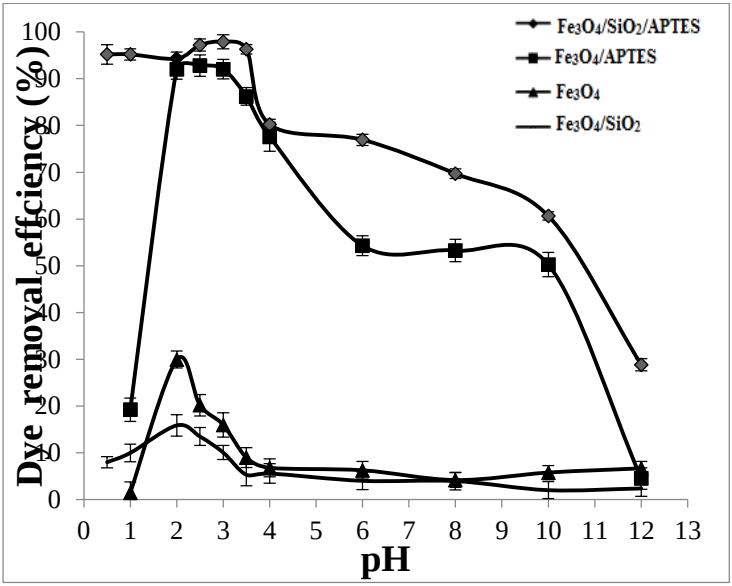

Fig.5: Comparison of adsorption capacities among building constituents of the adsorbent for adsorption of RR-120. Fe_3O_4/SiO_2/APTES (●); Fe_3O_4/APTES (■); Fe_3O_4 (▲); and Fe_3O_4/SiO_2 (─). Experimental conditions: nanoparticles dosage of 20.0 mg, initial dye concentration of 20 mg L^{-1}, stirring time of 10.0 minutes.

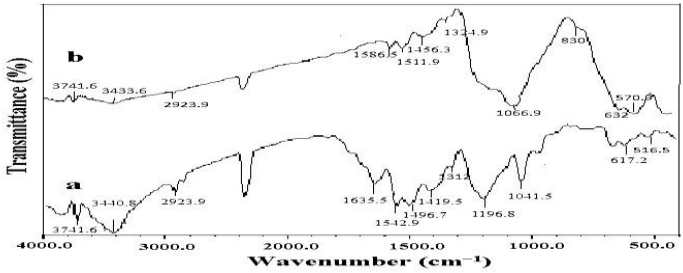

Fig.6: FTIR spectra of a, free Reactive Red 120 (RR-120); and b, RR-120 adsorbed on to Fe_3O_4/SiO_2/APTES nanoparticles.

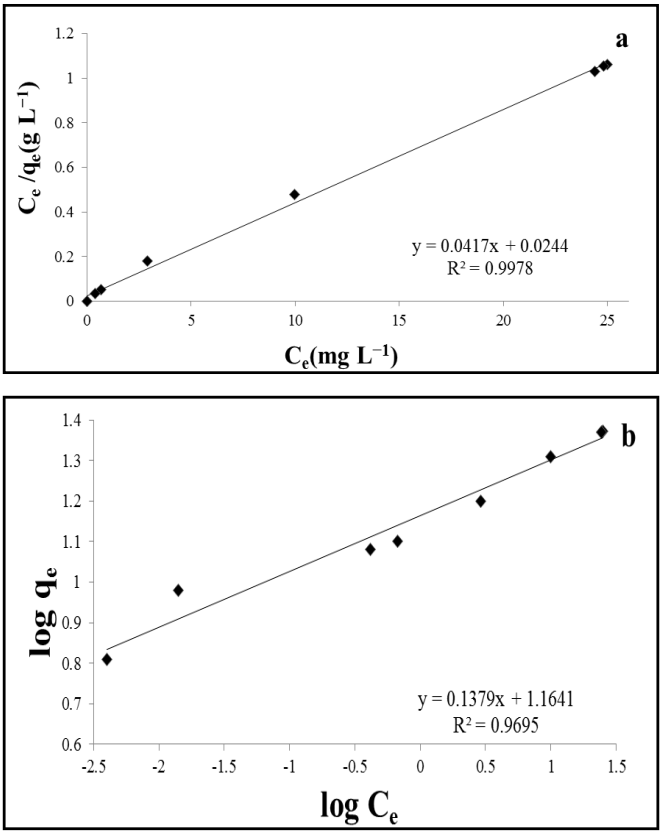

Journal of Applied Research in Chemistry

Volume2, Issue2 (Serial: 6), summer 2021

https://science-journals.ir

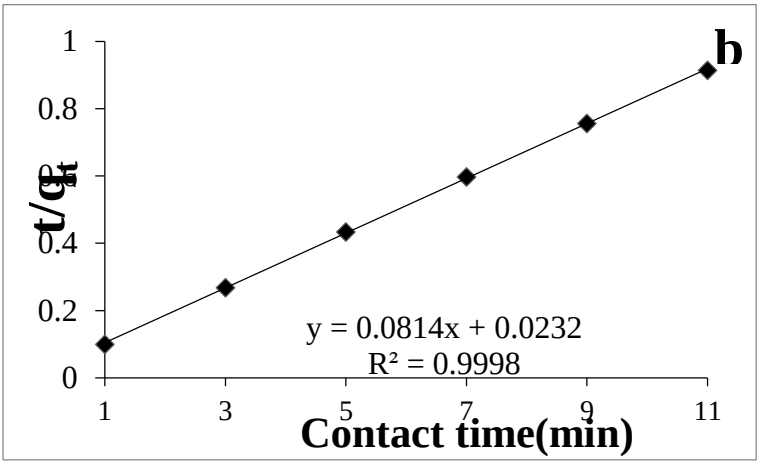

Fig.7: a, Langmuir isotherm plots; b, Freundlich isotherm plots for RR-120 adsorption onto Fe_3O_4/SiO_2/APTES nanoparticles. Experimental conditions: Fe_3O_4/SiO_2/APTES dosage of 5.0-30.0 mg, initial pH of 3.0, initial dye concentration of 45.0 mg L^{-1}, stirring time of 7.0 minutes.

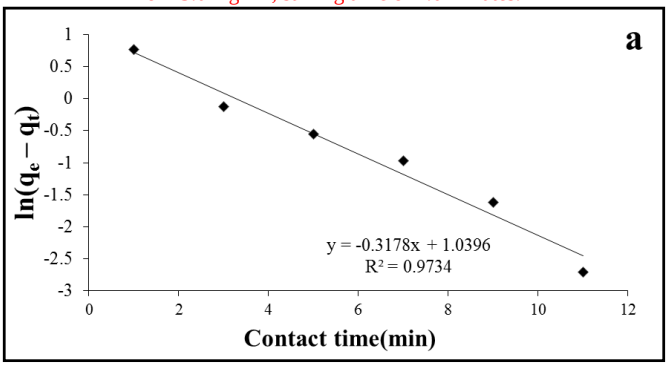

Fig.8: Plots of a, the pseudo-first-order rates; b, the pseudo-second-order rate for adsorption of RR-120 onto Fe_3O_4/SiO_2/APTES nanoparticles

References

[1] Poulios I., I. Aetopoulou, 1999. Photocatalytic degradation of the textile dye reactive orange 16 in the presence of TiO_2 suspensions. Environ. Technol. 20 (5): 479-487

[2] Vijayaraghavan K., Y.-S. Yun,2008. Biosorption of CI Reactive Black 5 from aqueous solution using acid-treated biomass of brown seaweed Laminaria sp. Dyes Pigm. 76 (3): 726-732.

[3] Moussavi G., M. Mahmoudi,2009. Removal of azo and anthraquinone reactive dyes from industrial wastewaters using MgO nanoparticles. J. Hazard. Mater. 168 (2): 806-812.

[4] Ozmen E. Y., M. Sezgin, A. Yilmaz, M. Yilmaz,2008. Synthesis of β-cyclodextrin and starch based polymers for sorption of azo dyes from aqueous solutions. Bioresour. Technol. 99 (3): 526-531.

[5] Afkhami A., R. Moosavi,2010. Adsorptive removal of Congo red, a carcinogenic textile dye, from aqueous solutions by maghemite nanoparticles. J. Hazard. Mater. 174 (1): 398-403.

[6] Kannan N., M. M. Sundaram, 2001. Kinetics and mechanism of removal of methylene blue by adsorption on various carbons-a comparative study. Dyes Pigm. 51 (1): 25-40.

[7] Wang S., H. Li, L. Xu, 2006. Application of zeolite MCM-22 for basic dye removal from wastewater. J. Colloid Interface Sci. 295 (1): 71-78.

[8] Arslan I., I. A. Balcioglu,2001. Degradation of Remazol Black B dye and its simulated dyebath wastewater by advanced oxidation processes in heterogeneous and homogeneous media. Color. Technol. 117 (1): 38-42.

[9] Gutierrez M., M. Pepio, M. Crespi,2002. Electrochemical oxidation of reactive dyes: method validation and application. Color. Technol. 118 (1): 1-5.

[10] Tsui S.-M., W. Chu, 2001. Photocatalytic degradation of dye pollutants in the presence of acetone. Water Sci. Technol. 44 (6): 173-180.

[11] Stolz A., 2001. Basic and applied aspects in the microbial degradation of azo dyes. Appl. Microbiol. Biot. 56 (1-2): 69-80.

[12] Bell J., C. A. Buckley, 2003. Treatment of a textile dye in the anaerobic baffled reactor. Water SA, 29 (2): 129-134.

[13] Haghighi-Podeh M. R., M. Sarhadi, S. M. Ghoreishi,2001. A combined chemical reduction and biological oxidation process for the treatment of textile wastewater. Water Qual. Res. J. Can. 36 (3): 605-617.

[14] Kapdan I. K., R. Ozturk,2005. Effect of operating parameters on color and COD removal performance of SBR: Sludge age and initial dyestuff concentration. J. Hazard. Mater. 123 (1): 217-222.

[15] Arıca M. Y., G. Bayramoğlu,2007. Biosorption of Reactive Red-120 dye from aqueous solution by native and modified fungus biomass preparations of Lentinus sajor-caju. J. Hazard. Mater. 149 (2): 499-507.

[16] Rizzo L., J. Koch, V. Belgiorno, M. Anderson,2007. Removal of methylene blue in a photocatalytic reactor using polymethylmethacrylate supported TiO_2 nanofilm. Desalination, 211 (1): 1-9.

[17] Kusvuran E., O. Gulnaz, S. Irmak, O. M. Atanur, H. I. Yavuz, O. Erbatur,2004. Comparison of several advanced oxidation processes for the decolorization of Reactive Red 120 azo dye in aqueous solution. J. Hazard. Mater. 109 (1): 85-93.K.

[18] Han R., D. Ding, Y. Xu, W. Zou, Y. Wang, Y. Li, L. Zou,2008. Use of rice husk for the adsorption of congo red from aqueous solution in column mode. Bioresour. Technol. 99 (8): 2938-2946.

[19] Papić S., N. Koprivanac, A. L. Božić, A. Meteš,2004. Removal of some reactive dyes from synthetic wastewater by combined Al (III) coagulation/carbon adsorption process. Dyes Pigm. 62 (3): 291-298.

[20] Hu Z., J. Zhang, W. Chan, Y. Szeto, 2006. The sorption of acid dye onto chitosan nanoparticles. Polymer, 47 (16): 5838-5842

[21] Nagappa B., G. Chandrappa,2007. Mesoporous nanocrystalline magnesium oxide for environmental remediation. Micropor. Mesopor. Mat. 106 (1): 212-218.

[22] Neppolian B., Q. Wang, H. Jung, H. Choi,2008. Ultrasonic-assisted sol-gel method of preparation of TiO_2 nano-particles: characterization, properties and 4-chlorophenol removal application. Ultrason. Sonochem. 15 (4): 649-658

[23] Zelmanov G., R. Semiat,2008. Iron (3) oxide-based nanoparticles as catalysts in advanced organic aqueous oxidation. Water Res. 42 (1): 492-498.

[24] Absalan G., M. Asadi, S. Kamran, L. Sheikhian, D. M. Goltz, 2011. Removal of reactive red-120 and 4-(2-pyridylazo) resorcinol from aqueous samples by Fe_3O_4 magnetic nanoparticles using ionic liquid as modifier. J. Hazard. Mater. 192 (2): 476-484.

[25] Madrakian T., A. Afkhami, M. Ahmadi, H. Bagheri,2011. Removal of some cationic dyes from aqueous solutions using magnetic-modified multi-walled carbon nanotubes. J. Hazard. Mater. 196 109-114.

[26] Dalvand A., R. Nabizadeh, M. R. Ganjali, M. Khoobi, S. Nazmara, A. H. Mahvi,2016. Modeling of Reactive Blue 19 azo dye removal from colored textile wastewater using L-arginine-functionalized Fe_3O_4 nanoparticles: Optimization, reusability, kinetic and equilibrium studies. J. Magn. Magn. Mater. 404 179-189.

[27] Xu H., Y. Zhang, Q. Jiang, N. Reddy, Y. Yang,2013. Biodegradable hollow zein nanoparticles for removal of reactive dyes from wastewater. J. Environ. Manage. 125 33-40.

[28] Faraji M., Y. Yamini, E. Tahmasebi, A. Saleh, F. Nourmohammadian,2010.Cetyltrimethylammonium bromide-coated magnetite nanoparticles as highly efficient adsorbent for rapid removal of reactive dyes from the textile companies' wastewaters. J. Iran. Chem. Soc. 7 (2): S130-S144.

[29] Chen D., Y. Li, J. Zhang, W. Li, J. Zhou, L. Shao, G. Qian,2012. Efficient removal of dyes by a novel magnetic Fe_3O/ZnCr-layered double hydroxide adsorbent from heavy metal wastewater. J. Hazard. Mater. 243 152-160

[30] Salem A.-N. M., M. Ahmed, M. El-Shahat,2016. Selective adsorption of amaranth dye on Fe_3O_4/MgO nanoparticles. J. Mol. Liq. 219 780-788.

[31] Yavari S., N. M. Mahmodi, P. Teymouri, B. Shahmoradi, A. Maleki, 2015. Cobalt ferrite nanoparticles: Preparation, characterization and anionic dye removal capability. J. Taiwan Inst. Chem. Eng. 59 320-329.

[32] Chikazumi S., S. Taketomi, M. Ukita, M. Mizukami, H. Miyajima, M. Setogawa, Y. Kurihara,1987. Physics of magnetic fluids. J. Magn. Magn. Mater. 65 (2-3): 245-251.

[33] Lu A. H., W. Schmidt, N. Matoussevitch, H. Bönnemann, B. Spliethoff, B. Tesche, E. Bill, W. Kiefer, F. Schüth,2004. Nanoengineering of a magnetically separable hydrogenation catalyst. Angew. Chem. 116 (33): 4403-4406.

[34] Tsang S. C., V. Caps, I. Paraskevas, D. Chadwick, D. Thompsett, 2004. Magnetically Separable, Carbon-Supported Nanocatalysts for the Manufacture of Fine Chemicals. Angew. Chem. 116 (42): 5763-5767.

[35] Gupta A. K., M. Gupta, 2005. Synthesis and surface engineering of iron oxide nanoparticles for biomedical applications. Biomaterials, 26 (18): 3995-4021Z.

[36] Mornet S., S. Vasseur, F. Grasset, P. Veverka, G. Goglio, A. Demourgues, J. Portier, E. Pollert, E. Duguet,2006. Magnetic nanoparticle design for medical applications. Prog. Solid State Chem. 34 (2): 237-247.

[37] Li Z., L. Wei, M. Gao, H. Lei,2005. One-Pot Reaction to Synthesize Biocompatible Magnetite Nanoparticles. Adv. Mater. 17 (8): 1001-1005.

[38] Hyeon T., 2003. Chemical synthesis of magnetic nanoparticles. Chem. Commun. (8): 927-934

[39] Elliott D. W., W.-X. Zhang, 2001. Field assessment of nanoscale bimetallic particles for groundwater treatment. Environ. Sci. Technol. 35 (24): 4922-4926

[40] Takafuji M., S. Ide, H. Ihara, Z. Xu,2004. Preparation of poly (1-vinylimidazole)-grafted magnetic nanoparticles and their application for removal of metal ions. Chem. Mater. 16 (10): 1977-1983.

[41] Meybeck M.,2003. Global analysis of river systems: from Earth system controls to Anthropocene syndromes. Philos. Trans. R. Soc. Lond. B Biol. Sci. 358 (1440): 1935-1955.

[42] L. Rassaei, F. Marken, M. Sillanpää, M. Amiri, C. M. Cirtiu, and M. Sillanpää, "Nanoparticles in electrochemical sensors for environmental monitoring," TrAC Trends in Analytical Chemistry, vol. 30, no. 11, pp. 1704–1715, 2011.

[43] Liu X., Y. Guan, Z. Ma, H. Liu,2004. Surface modification and characterization of magnetic polymer nanospheres prepared by miniemulsion polymerization. Langmuir, 20 (23): 10278-10282.

[44] Kim D. K., M. Mikhaylova, F. H. Wang, J. Kehr, B. Bjelke, Y. Zhang, T. Tsakalakos, M. Muhammed,2003. Starch-coated superparamagnetic nanoparticles as MR contrast agents. Chem. Mater. 15 (23): 4343-4351.

[45] Sun Y., L. Duan, Z. Guo, Y. DuanMu, M. Ma, L. Xu, Y. Zhang, N. Gu,2005. An improved way to prepare superparamagnetic magnetite-silica core-shell nanoparticles for possible biological application. J. Magn. Magn. Mater. 285 (1): 65-70.

[46] Zhang L., B. Liu, S. Dong, 2007. Bifunctional nanostructure of magnetic core luminescent shell and its application as solid-state electrochemiluminescence sensor material. J. Phys. Chem. B 111 (35): 10448-10452.

[47] Yamaura M., R. Camilo, L. Sampaio, M. Macedo, M. Nakamura, H. Toma,2004. Preparation and characterization of (3-aminopropyl) triethoxysilane-coated magnetite nanoparticles. J. Magn. Magn. Mater. 279 (2): 210-217.

[48] Feng B., R. Hong, L. Wang, L. Guo, H. Li, J. Ding, Y. Zheng, D. Wei,2008. Synthesis of Fe_3O_4/APTES/PEG diacid functionalized magnetic nanoparticles for MR imaging. Colloids Surf. A 328 (1): 52-59.

[49] Kim D., Y. Zhang, W. Voit, K. Rao, M. Muhammed,2001. Synthesis and characterization of surfactant-coated superparamagnetic monodispersed iron oxide nanoparticles. J. Magn. Magn. Mater. 225 (1): 30-36.

[50] Chang J. H., K. H. Kang, J. Choi, Y. K. Jeong,2008. High efficiency protein separation with organosilane assembled silica coated magnetic nanoparticles. Superlattices Microstruct. 44 (4): 442-448.

[51] Ma M., Y. Zhang, W. Yu, H.-y. Shen, H.-q. Zhang, N. Gu,2003. Preparation and characterization of magnetite nanoparticles coated by amino silane. Colloids Surf., A 212 (2): 219-226.

[52] Ng C., J. N. Losso, W. E. Marshall, R. M. Rao,2002. Freundlich adsorption isotherms of agricultural by-product-based powdered activated carbons in a geosmin–water system. Bioresour. Technol. 85 (2): 131-135.

[53] Chun J. H., S. K. Jeon, N. Y. Kim, J. Y. Chun,2005. The phase-shift method for determining Langmuir and Temkin adsorption isotherms of over-potentially deposited hydrogen for the cathodic H_2 evolution reaction at the poly-Pt/H_2SO_4 aqueous electrolyte interface. Int. J. Hydrogen Energy, 30 (13): 1423-1436.

[54] Freundlich H., 1906. Over the adsorption in solution. J. Phys. Chem. 57 (385): e470.

[55] Langmuir I.,1918. The adsorption of gases on plane surfaces of glass, mica and platinum. J. Am. Chem. Soc. 40 (9): 1361-1403.

[56] O'Connor T. P., J. Mueller,2001. Modeling competitive adsorption of chlorinated volatile organic

[57] Redlich O., D. L. Peterson, 1959. A useful adsorption isotherm. J. Phys. Chem. 6

[58] Waldron R., 1955. Infrared spectra of ferrites. Phys. Rev. 99 (6): 1727.Redlich O., D. L. Peterson,1959. A useful adsorption isotherm. J. Phys. Chem. 63 (6): 1024-1024.

[59] Park S., J. Kim, J. Lim, C. Kim, 2008. Surface-modified magnetic nanoparticles with lecithin for applications in biomedicine. Curr. Appl. Phys. 8 (6): 706-709

[60] Faivre D., P. Zuddas, 2006. An integrated approach for determining the origin of magnetite nanoparticles. Earth Planet. Sci. Lett. 243 (1): 53-60.

[61] Can K., M. Ozmen, M. Ersoz, 2009. Immobilization of albumin on aminosilane modified superparamagnetic magnetite nanoparticles and its characterization. Colloids Surf. B 71 (1): 154-159.

[62] Park M. E., J. H. Chang, 2007. High throughput human DNA purification with aminosilanes tailored silica-coated magnetic nanoparticles. Mater. Sci. Eng. C 27 (5): 1232-1235

[63] Uddin M. T., M. A. Islam, S. Mahmud, M. Rukanuzzaman,2009. Adsorptive removal of methylene blue by tea waste. J. Hazard. Mater. 164 (1): 53-60.

[64] Zargar B., H. Parham, A. Hatamie,2009. Modified iron oxide nanoparticles as solid phase extractor for spectrophotometeric determination and separation of basic fuchsin. Talanta, 77 (4): 1328-1331.

[65] Laurent S., D. Forge, M. Port, A. Roch, C. Robic, L. Vander Elst, R. N. Muller,2008. Magnetic iron oxide nanoparticles: synthesis, stabilization, vectorization, physicochemical characterizations, and biological applications. Chem. Rev. 108 (6): 2064-2110.

[66] Hu Y., T. Guo, X. Ye, Q. Li, M. Guo, H. Liu, Z. Wu,2013. Dye adsorption by resins: effect of ionic strength on hydrophobic and electrostatic interactions. Chem. Eng. J. 228 392-397.

[67] Paul J., A. A. Kadam, S. P. Govindwar, P. Kumar, L. Varshney,2013. An insight into the influence of low dose irradiation pretreatment on the microbial decolouration and degradation of reactive red-120 dye. Chemosphere, 90 (4): 1348-1358.